Available online at www.sciencedirect.com

ScienceDirect

journal homepage: www.elsevier.com/locate/he

Tuning the microstructure of organosilica membranes with improved gas permselectivity via the co-polymerization of 1,2-bis(triethoxysilyl) ethane and 1,2-bis(triethoxysilyl)methane

Hengfei Zhang [a], *Die He* [a], *Shufeng Niu* [b], *Hong Qi* [a,*]

[a] *State Key Laboratory of Material-Oriented Chemical Engineering, Membrane Science and Technology Research Center, Nanjing Tech University, Nanjing, 210009, China*

[b] *Hongyi Ceramic Membranes Research Institute, Nanjing Hongyi Ceramic Nanofiltration Membranes Co., Ltd., Nanjing, 210009, Jiangsu, China*

HIGHLIGHTS

- BTESE-BTESM membranes were prepared by using the sol-gel method.
- BTESM has significant influence on the BTESE-BTESM networks.
- E-M-3:7 membrane exhibited the optimal H_2/CO_2 separation performance.

GRAPHICAL ABSTRACT

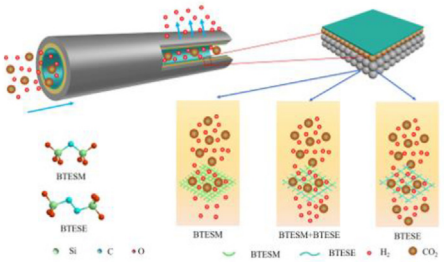

ARTICLE INFO

Article history:
Received 20 December 2020
Received in revised form
31 January 2021
Accepted 17 February 2021
Available online xxx

Keywords:
Hydrogen
Organosilica
Separation
Co-polymerization
Membranes

ABSTRACT

1,2-bis(triethoxysilyl)ethane (BTESE)-derived membranes have proven thermal and hydrothermal stability and molecular sieving properties. However, BTESE-derived membranes still have low gas permselectivity due to their loose structure. Herein, we propose a novel strategy of co-polymerization using precursors of both BTESE and 1,2-bis(triethoxysilyl)methane (BTESM) to improve the gas permselectivity of BTESE-derived membranes. BTESM is introduced into BTESE network and the microstructure can be adjusted by different molar ratios of BTESE to BTESM. We find that, as the content of BTESM increase, H_2 permeations of BTESE-BTESM membranes remain nearly constant, while the permeations of larger gases (CO_2 and N_2 etc.) exhibit a greatly decreased. The membrane with a molar ratio of BTESE:BTESM = 3:7 exhibits the highest H_2/CO_2 (11.3) and H_2/N_2 (26.8) permselectivity while having a relatively high H_2 permeance (1.52×10^{-6} mol m^2 s^{-1}·Pa^{-1}). Our findings may provide novel insights into preparation of

* *Corresponding author.*
E-mail addresses: zhanghengfei@njtech.edu.cn (H. Zhang), hqi@njtech.edu.cn (H. Qi).

https://doi.org/10.1016/j.ijhydene.2021.02.139

co-polymerization organosilica membranes with excellent H_2/CO_2 and H_2/N_2 separation performance.

Introduction

The family of organosilica membranes includes numerous members due to the various organoalkoxysilane precursors with tunable organic group linkages [1,2]. According to the different positions of organic groups (R) in the organosilica networks, the organoalkoxysilane precursors can be divided into two types: (1) the bridging position type (Si-R-Si) and (2) the terminal position type (Si-R), both of which are presented in Fig. 1 [3]. Organic groups of the bridging type can be regarded as "spacers" between Si atoms which are part of the backbone in organosilica networks. Generally, the incorporation of a bridging R can expand the pore size due to the longer Si–C bonds (Si–C 1.97 Å, Si–O 1.57–1.59 Å) [4]. The terminal organic groups are similar to the pendants in the organosilica network as they cannot act as spacers and easily fill up the pores of membranes [1,3]. On the other hand, the organic groups exist in the branch chain and the composition of the backbone are still Si–O–Si groups which are easily attacked by water molecules [5,6]. Therefore, the hydrothermal stability of the terminal type of precursors derived organosilica membranes are not satisfied.

Multifarious organic bridging groups, including alkylene (e.g., CH_2, C_2H_4, C_6H_{12} and C_8H_{16}) and aromatic (e.g., benzene and biphenyl) groups present organosilica membranes with tailoring pore structure properties [7]. In particular, 1,2-bis(-triethoxysilyl)ethane (BTESE) with ethylene bridging groups between two Si atoms (Si–CH_2–CH_2–Si) is the most extensive research object belonging to the organosilica membrane family [8–14]. BTESE-derived membranes show well-known significant advantages, including the thermal and hydrothermal stability and favorable molecule separation performance in the applications of pervaporation, reverse osmosis, nanofiltration and gas separation [15–19]. However, in gas separation, BTESE-derived membranes show exceptionally low H_2/CO_2 and H_2/N_2 permselectivity. This disadvantage is ascribed to the larger pore size caused by the longer Si–C–C–Si bonds in the BTESE-derived network [20]. Therefore, tuning the microporous structures of BTESE-derived membranes to improve the gas permselectivity have attracted recent interest among researchers.

Co-polymerization of precursors is an effective method to tuning the microstructure of organosilica membranes at the molecular level [21–24]. Meng et al. [21] prepared organosilica membranes via the co-polymerization of mixed BTESE and tetraethyl orthosilicate (TEOS, Si–O–Si) precursors. They found that the order of the membrane pore size was BTESE > BTESE-TEOS > TEOS and that membrane pore size was dependent on the different minimum units of precursors. Compared with pure BTESE and TEOS derived membranes, BTESE-TEOS membranes have moderate microstructures which present a more balanced gas permeance and selectivity. However, it is evident that TEOS-derived membranes have poor hydrothermal stability. The incorporation of the Si–O–Si bonds into the BTESE network is bound to decrease the hydrothermal stability of BTESE-derived membranes. Chai et al. [23] investigated gas separation performance of mixed BTESE and methyltriethoxysilane (MTES, ≡Si–CH_3) derived membranes. The structures of BTESE-MTES hybrid membranes can be adjusted by tuning the molar ratios of BTESE to that of MTES. When the proportion of MTES was below 50% in the BTESE-MTES networks, the space of the pores were occupied by the terminal methyl groups, which caused the decreased pore volume and low gas permeance.

Herein, a novel method of tailoring the microstructure of organosilica membranes via the co-polymerization of BTESE and BTESM (Si–CH_2–Si) is introduced. The chemical structures of BTESM and BTESE are presented in Fig. 2. We believe that the introduction of the shorter Si–CH_2–Si groups into the BTESE network could decrease the pore size of BTESE-derived membranes, and further to improve their gas selectivity. In comparison to the precursor of TEOS, BTESM shows better hydrothermal stability because of its organic group linkage. On the other hand, BTESM belongs to the bridging type

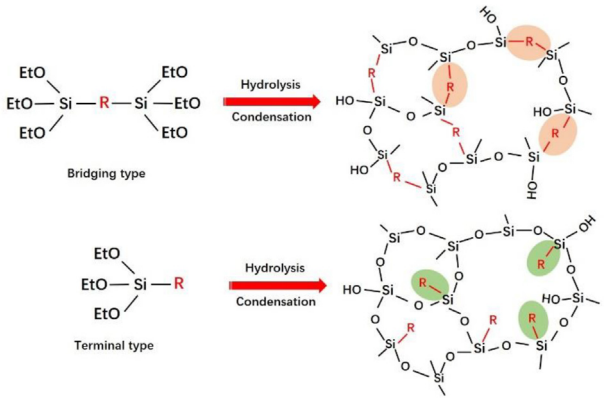

Fig. 1 – Schematic illustration of bridging and terminal type organoalkoxysilane precursors and their derived organosilica networks (R represents the organic groups).

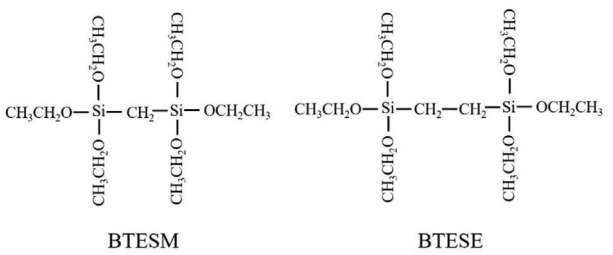

Fig. 2 – Chemical structures of BTESM and BTESE.

Please cite this article as: Zhang H et al., Tuning the microstructure of organosilica membranes with improved gas permselectivity via the co-polymerization of 1,2-bis(triethoxysilyl)ethane and 1,2-bis(triethoxysilyl)methane, International Journal of Hydrogen Energy, https://doi.org/10.1016/j.ijhydene.2021.02.139

precursor which will not fill up the pores of organosilica membranes. Based on these reasons, BTESM was selected as a precursor to co-polymerized with BTESE. In the present study, a series of co-polymerization sols with different molar ratios of BTESE to BTESM were synthesized. BTESE-BTESM membranes were fabricated based on these polymeric sols. The properties of the hybrid silica membranes, such as microstructures and six single gas permeances (He, H_2, CO_2, N_2, CH_4, and SF_6) were investigated in detail. This work may provide insights into tuning the microstructures of organosilica membranes via co-polymerization routes.

Materials and methods

Synthesis of BTESE-BTESM sols

2.5 mL BTESE (purity 97%, ABCR), 2.4 mL BTESM (purity 97%, ABCR) and 20 mL anhydrous ethanol (EtOH, purity 99.9%, Merck) were first mixed in an ice bath. Then, a mixture of 5 mL EtOH, 5 mL deionized (DI) water (5 μS cm^{-1} at 25 °C) and 0.5 mL hydrochloric acid solution (HCl, 1 mol L^{-1}) was added dropwise into the BTESE-BTESM mixture. Finally, the BTESE-BTESM-containing mixture was refluxed at 60 °C for 90 min to obtain the BTESE-BTESM sols. The molar ratio of the as-prepared sols is n(Si):n(EtOH):n(H_2O):n(H^+) = 1:31.7:22.2:0.04, among which the molar ratio of BTESE to BTESM is 5:5 (marked as E-M-5:5). By changing the molar ratios of BTESE to BTESM, five types of sols were synthesized as follows: 10:0 (BTESE), 8:2 (E-M-8:2), 5:5 (E-M-5:5), 3:7 (E-M-3:7) and 0:10 (BTESM).

Preparation of BTESE-BTESM membranes

To prepare the BTESE-BTESM membranes, the as-prepared sols were diluted to a solution of 0.2 M Si in concentration. Then, the diluted sols were coated onto inner side of hand-made tubular γ-Al_2O_3 mesoporous membranes (pore size: 5 nm, outer diameter: 12 mm, inner diameter: 8 mm, length: 50 mm) by the dip coating technique (temperature: 25 °C, withdrawal rate: 0.5 cm·min^{-1}, immersion time: 5 s). The freshly coated BTESE-BTESM membranes were dried in a humidity chamber (C4-180, Vötsch, 40 °C, 25% relative humidity) for 1 h. Finally, the membranes were calcined in the presence of N_2 atmosphere at 400 °C for 3 h in a tube furnace (GHA 12/1050, Carbolite).

BTESE-BTESM sols were dried at room temperature (25 °C) for 24 h to prepare xerogels. The obtained xerogels were ground into fine powders by using an agate mortar. The fine powders were calcined at the same conditions as the preparation of BTESE-BTESM membranes. The obtained BTESE-BTESM powders were used for characterization of the properties of the corresponding membranes.

Characterization

The particle size distribution of as-prepared sols was measured by a dynamic light scattering analyzer (Zetasizer Nano ZS90, Malvern). Fourier transform infrared (FTIR) spectroscopy (NICOLET 8700, Thermo Nicolet Corporation) was used to analyze the chemical compositions of BTESE-BTESM powders. Thermogravimetric analysis (TGA) was used to evaluate the content of organic groups in a N_2 atmosphere heating from room temperature (25 °C) to 800 °C. The surface and cross-sectional morphologies of membranes were observed using scanning electron microscopy (SEM, S-4800, Hitachi). The tubular membranes were cut into small pieces, followed by fixing them on the electron microscope platform horizontally and vertically with conductive adhesive, respectively. The microstructures of the as-prepared BTESE-BTESM membranes were evaluated by characterizing their corresponding powders through N_2 adsorption-desorption isotherms (ASAP 2020, Micromeritics). Before measurement, samples were degassed under vacuum at 200 °C for 12 h. Pore size distributions of the as-prepared powders were calculated by the non-local density functional theory method (NLDFT).

Evaluation of gas separation performance

The single gas permeances of He, H_2, CO_2, N_2, CH_4, and SF_6 were measured at 200 °C on a home-made apparatus (Fig. 3). The gas permeance was calculated according to Eq. (1):

$$P_i = \frac{F_i}{A\,\Delta P} \tag{1}$$

where P_i is the permeance of gas i (mol·m^{-2} s^{-1} Pa^{-1}), F_i is the flow rate (mol·s^{-1}), A is the effective membranes area (m^2) and ΔP is the transmembrane pressure (Pa).

The ideal separation factor (α) was calculated by Eq. (2):

$$\alpha = \frac{P_i}{P_j} \tag{2}$$

where P_i and P_j are the permeance of gas i and j, respectively.

Results and discussion

Particle size distributions of organosilica sols

The BTESE-BTESM sols were synthesized by the polymeric route which is an acid-catalyzed simultaneous hydrolysis and condensation reaction. This reaction can be described as following [19,25]:

Hydrolysis

$$R-Si(OC_2H_5)_{3-n}(OH)_n + H_2O \xrightarrow{H^+} R-Si(OC_2H_5)_{2-n}(OH)_{n+1} + C_2H_5OH \tag{3}$$

Condensation

$$R-Si(OC_2H_5)_{2-n}(OH)_{n+1} + R'-Si(OC_2H_5)_{2-m}(OH)_{m+1} \rightarrow R-Si(OC_2H_5)_{2-n}(OH)_n - Si-O-Si-(OC_2H_5)_{2-m}(OH)_m R' + H_2O \tag{4}$$

where R and R′ are the organic groups linkages, n and m can be 0, 1 or 2.

Fig. 4 shows the particle size distributions of BTESE-BTESM sols measured by a dynamic light scattering analyzer. The homogeneous organosilica sols with the Tyndall effect were obtained. The particle size distributions of BTESE-BTESM sols range from 3 to 10 nm. The average particle sizes of the as-prepared sols are approximately 5 nm which has a good

Please cite this article as: Zhang H et al., Tuning the microstructure of organosilica membranes with improved gas permselectivity via the co-polymerization of 1,2-bis(triethoxysilyl)ethane and 1,2-bis(triethoxysilyl)methane, International Journal of Hydrogen Energy, https://doi.org/10.1016/j.ijhydene.2021.02.139

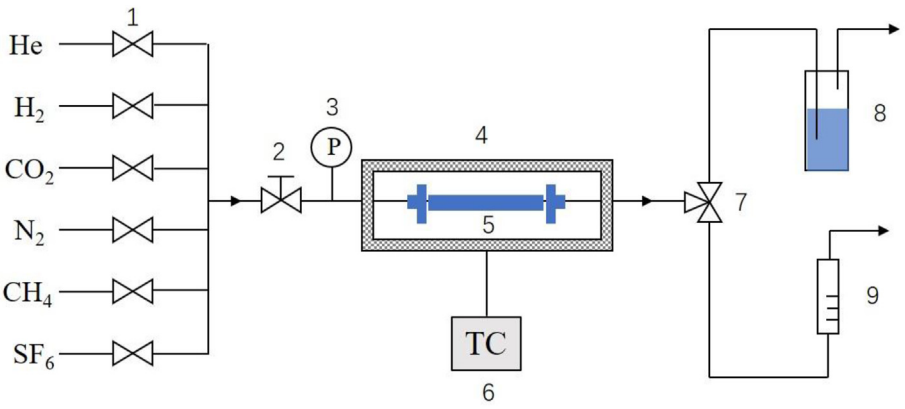

Fig. 3 – Experimental apparatus for single gas permeation. 1. Stop valve 2. Pressure controller 3. Pressure gauge 4. Electric furnace 5. Membrane module 6. Temperature controller 7. Three-way valve 8. Gas washing 9. Soap film meter.

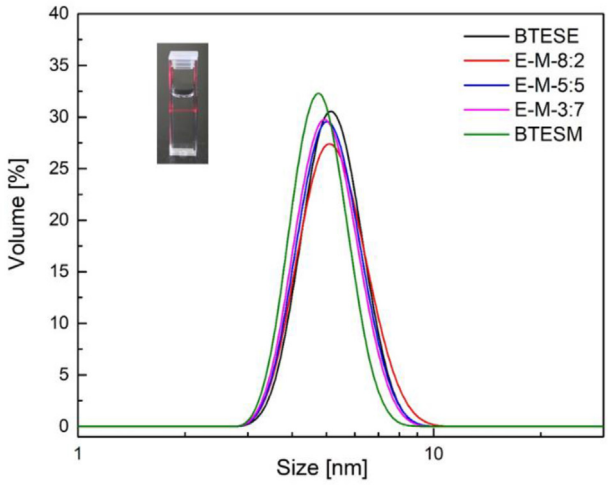

Fig. 4 – Particle size distributions of BTESE-BTESM sols.

match with the support proved by our previous work [19]. It should be noted that the average particle sizes of BTESE-BTESM sol slightly decrease as the proportion of BTESM increased. This result may be ascribed to the shorter linkage of BTESM which caused the smaller particle sizes, when BTESM was introduced into the BTESE sol.

Chemical composition analysis of BTESE-BTESM membranes

Fig. 5a shows the TGA curves of BTESE-BTESM gels measured under a N_2 atmosphere heating from room temperature (25 °C) to 800 °C. The TGA curves of all samples showed the three-stage mass loss. The first mass loss from 25 to 200 °C occurs through the process of dehydration and dissolvent. Next, as the temperature increased from 200 to 550 °C, the polymerization of Si–OH occurs which results in the formation of Si–O–Si bonds. Finally, the organic groups in the organosilica networks start to decompose when the temperature reaches 550 °C [26]. The mass loss of organic groups of the five samples are given in Fig. 5b and it is defined as the sample mass measured at 550 °C subtracts the same samples measured at 800 °C. The mass loss of organic groups was in the order of BTESE > E-M-8:2 > E-M-5:5 > E-M-3:7>BTESM. Because, the mass of bridged organic groups (–CH_2–CH_2-) in the BTESE network is larger than that of bridged organic groups (–CH_2–) in BTESM network. When the temperature reaches the decomposition temperature of organic components, BTESE gel will lose more mass than BTESM gel. The decreased mass loss of organic groups can indirectly prove that BTESM was successfully introduced into the structure of BTESE.

FTIR spectra were used to analyze the chemical compositions of BTESE-BTESM powders. Fig. 6a shows the FTIR spectra of all samples are similar. The peaks at 3450, 16,28 and 1045 cm^{-1} are assigned to the mobile Si–OH stretching vibrations, H_2O deformation vibration and Si–O–Si asymmetric stretching vibrations, respectively [27,28]. It can be clearly seen from Fig. 6b that BTESE and BTESM samples have a peak at 1417 and 1366 cm^{-1} that are assigned to the - CH_2–CH_2- and –CH_2- groups, respectively [27,29]. The intensity of the –CH_2-CH_2-group gradually decreased as the proportion of BTESE decreased. This result is consistent with the TGA analysis, further confirming BTESM was successfully introduced into BTESE network.

Morphological and structural analysis of BTESE-BTESM membranes

N_2 adsorption-desorption experiments were conducted to determine the effects of the co-polymerization of BTESE and BTESM on the microstructural changes of organosilica networks. Fig. 7a shows the N_2 adsorption-desorption isotherms of BTESE-BTESM powders. Obviously, all samples reached high N_2 adsorption capacities rapidly at a very low relative pressure region, which matches well with the characteristics of type I isotherms, confirming that BTESE-BTESM membranes have microporous structures [30]. The detailed microstructure information.

(Brunauer-Emmett-Teller surface area (S_{BET}), Pore volume (V_p)) are given in Table 1. BTESE powder showed the highest S_{BET} (329 $m^2\ g^{-1}$) and largest V_p (0.176 $cm^3\ g^{-1}$) due to its loose structure. It is noteworthy that S_{BET} and V_p of BTESE-BTESM powders decreased as the proportion of BTESM increased, and BTESM powder showed the lowest S_{BET} (157 $m^2\ g^{-1}$) and

Please cite this article as: Zhang H et al., Tuning the microstructure of organosilica membranes with improved gas permselectivity via the co-polymerization of 1,2-bis(triethoxysilyl)ethane and 1,2-bis(triethoxysilyl)methane, International Journal of Hydrogen Energy, https://doi.org/10.1016/j.ijhydene.2021.02.139

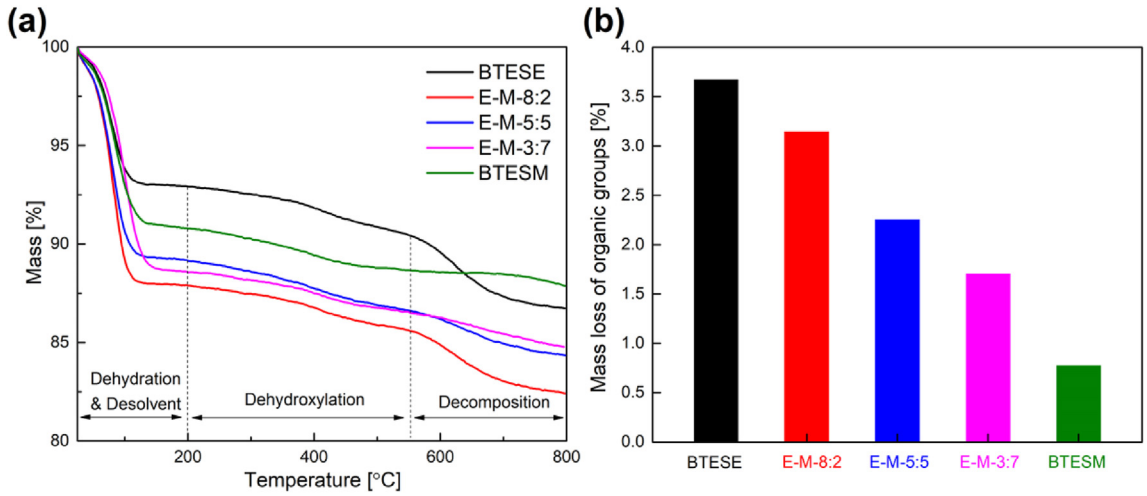

Fig. 5 – (a) TGA curves of BTESE-BTESM gels and (b) mass loss of organic groups.

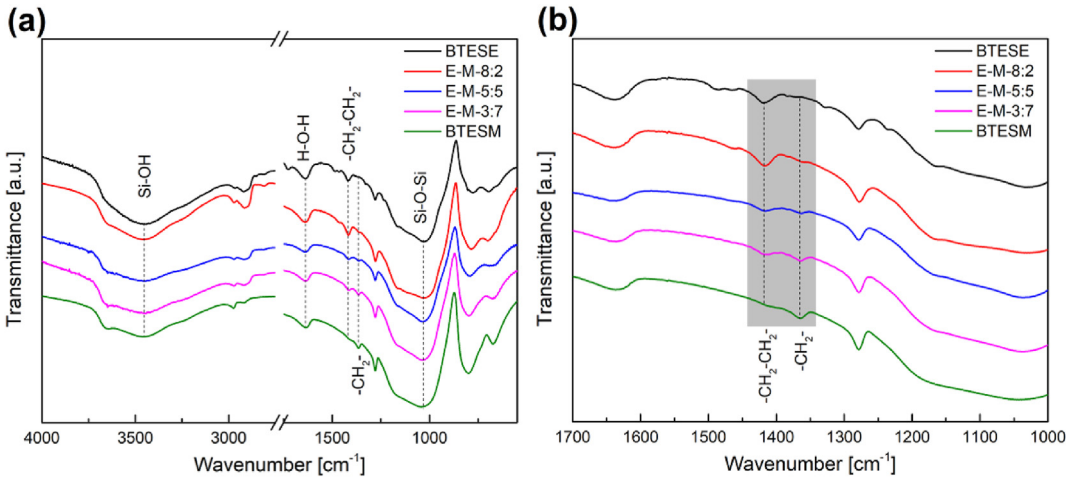

Fig. 6 – (a) FTIR spectra of BTESE-BTESM powders and (b) the enlarged view from 1700 to 1000 wavenumber cm^{-1}.

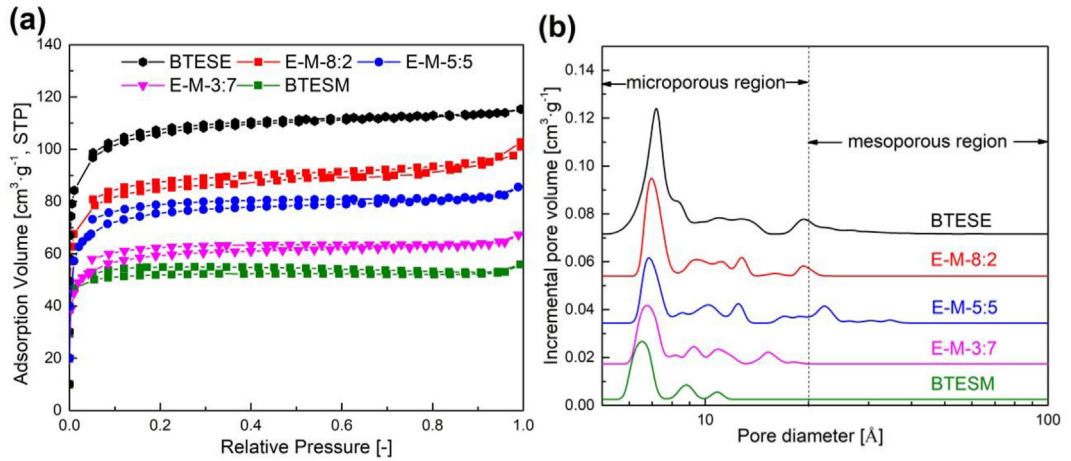

Fig. 7 – (a) N_2 adsorption-desorption isotherms and (b) pore size distributions of BTESE-BTESM powders.

smallest V_p (0.082 $cm^3\ g^{-1}$). This result can be ascribed to the shorter organic linkage of BTESM which caused the structure of BTESE-BTESM networks dense. To further explore the porous structures of the as-prepared powders, the pore size distributions of BTESE-BTESM powders were calculated based on the NLDFT method (Fig. 7b). The pore size distributions of

Please cite this article as: Zhang H et al., Tuning the microstructure of organosilica membranes with improved gas permselectivity via the co-polymerization of 1,2-bis(triethoxysilyl)ethane and 1,2-bis(triethoxysilyl)methane, International Journal of Hydrogen Energy, https://doi.org/10.1016/j.ijhydene.2021.02.139

Table 1 – Pore structure data of BTESE-BTESM powders.

Samples	S_{BET} ($m^2 \cdot g^{-1}$)	V_{total} ($cm^3 \cdot g^{-1}$)
BTESE	329	0.176
E-M-8:2	261	0.154
E-M-5:5	237	0.132
E-M-3:7	186	0.104
BTESM	157	0.082

Note: S_{BET} and V_{total} represent Brunauer-Emmett-Teller (BET) surface area and total pore volume, respectively.

BTESE, E-M-8:2, E-M-5:5, E-M-3:7 and BTESM networks were centered at 7.19, 6.98, 6.84, 6.75 and 6.54 Å, respectively. The decreased S_{BET}, V_p and pore size demonstrate that the introduction of BTESM can effectively tune the microstructure of BTESE networks.

Fig. 8 shows the surface and cross-sectional morphologies of the as-prepared BTESE-BTESM membranes. The BTESE membrane has a smooth and defect-free surface, and an asymmetric structure including a α-Al_2O_3 support, a γ-Al_2O_3 intermedia layer and a BTESE top layer. All the BTESE-BTESM membranes exhibited a thin separation layer with the similar thickness of 100 nm.

Gas separation performance of BTESE-BTESM membranes

Six gas molecules with different kinetic diameters (dHe = 2.6 Å, $d$$H_2$ = 2.89 Å, $d$$CO_2$ = 3.3 Å, $d$$N_2$ = 3.64 Å, $d$$CH_4$ = 3.82 Å, $d$$SF_6$ = 5.5 Å) were used to characterize the gas separation performance of BTESE-BTESM membranes. Fig. 9a shows the gas permeances of γ-Al_2O_3 support and BTESE-BTESM membranes measured at 200 °C. It was found that all the as-prepared membranes have a lower gas permeance compared with γ-Al_2O_3 support. The gas permeance of all the membranes exhibited a decreasing tendency as the kinetic diameter of gases increases, proving their molecular sieving properties [31]. As the proportion of BTESM increased, the gas permeance of BTESE- BTESM membranes decreased. To compare the gas permeance and permselectivity of BTESE-BTESM membranes in more detail, the H_2 permeance, H_2/CO_2 and H_2/N_2 ideal permselectivity were evaluated and are given in Fig. 9b. BTESE membrane has the highest H_2 permeance of 3.58×10^{-6} mol m^2 $s^{-1} \cdot Pa^{-1}$, but the H_2/CO_2 (5.7) and H_2/N_2 (8) ideal permselectivity are lowest due to the loose structure and larger pore size of the membrane. Interestingly, as the proportion of BTESM increased from 20% to 70%, the H_2 permeance of the BTESE-BTESM membrane maintained at a relatively high value, while the H_2/CO_2 and H_2/N_2 permselectivity increased. The reason is that when BTESM was introduced into BTESE network, the numbers of large pores decreased, but the numbers of small pores increased. Therefore, as the BTESM content increase, the decreased pore size of BTESE-BTESM membranes will block the transportation of gases provided with large kinetic diameter, such as CO_2, N_2, CH_4 and SF_6. While little effect can be found on transportation of He and H_2 through those membranes. As a result, the E-M-3:7 membrane showed the highest H_2/CO_2 (11.3) and H_2/N_2 (26.8) permselectivity which are much higher than the associated Knudsen diffusion factor (H_2/CO_2 = 4.7H_2/N_2 = 3.7). Meanwhile, the H_2 permeance of the E-M-3:7 membrane remained relatively high with a permeance of 1.52×10^{-6} mol m^2 $s^{-1} \cdot Pa^{-1}$. This result indicated that the co-polymerization of BTESE and BTESM is an effective method to improve the H_2/CO_2 permselectivity without the cost of the reduced the H_2 permeance.

According to the aforementioned results of chemical composition, microstructure, and singe gas permeance, the hypothetical structures of pure BTESM, BTESE-BTESM and pure BTESE membranes are schematically illustrated in Fig. 10. The BTESM membrane has a denser structure resulting in the low H_2 permeance. On the contrary, the BTESE membrane shows the high H_2 permeance due to the loose structure

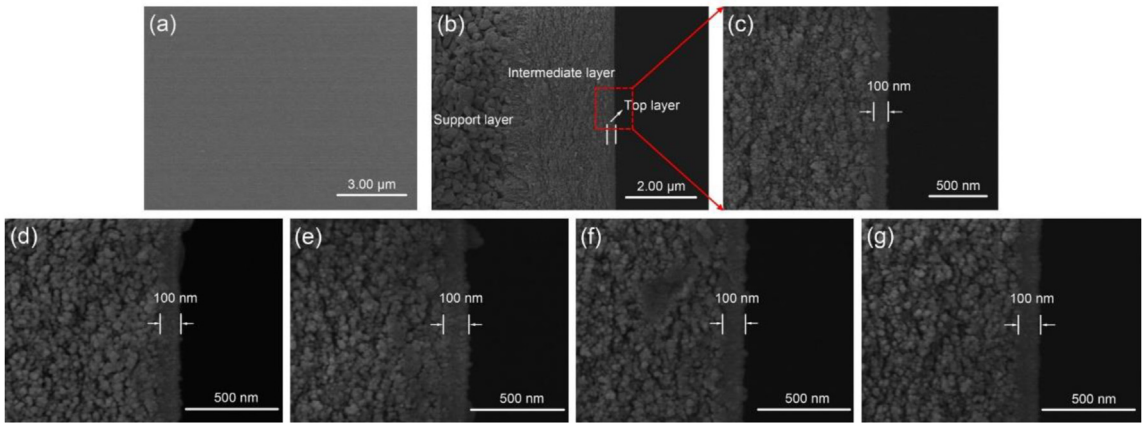

Fig. 8 – SEM images (a)–(c) surface and cross-section of BTESE membranes, (d)–(g) cross-sections of E-M-8:2, E-M-5:5, E-M-3:7 and BTESM membranes, respectively.

Please cite this article as: Zhang H et al., Tuning the microstructure of organosilica membranes with improved gas permselectivity via the co-polymerization of 1,2-bis(triethoxysilyl)ethane and 1,2-bis(triethoxysilyl)methane, International Journal of Hydrogen Energy, https://doi.org/10.1016/j.ijhydene.2021.02.139

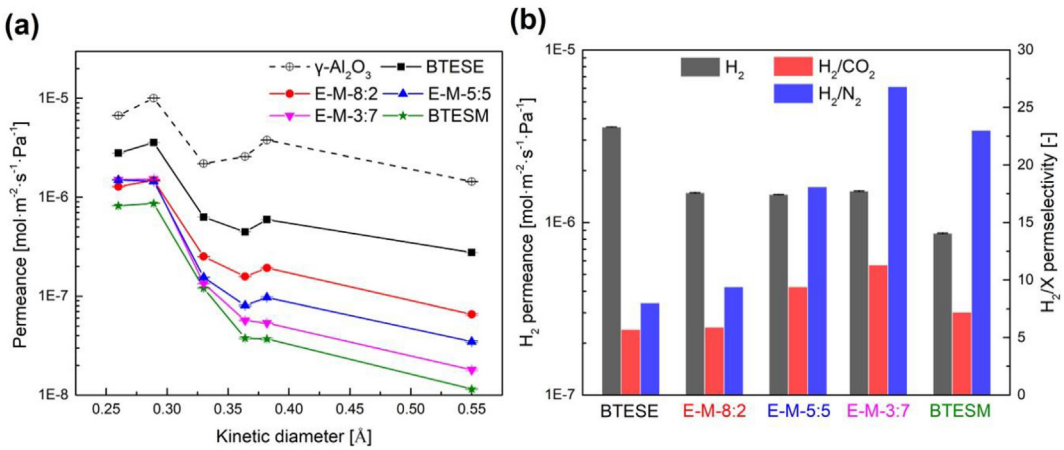

Fig. 9 – Gas permeance (a) and gas permselectivities (b) of BTESE-BTESM membranes measured at 200 °C.

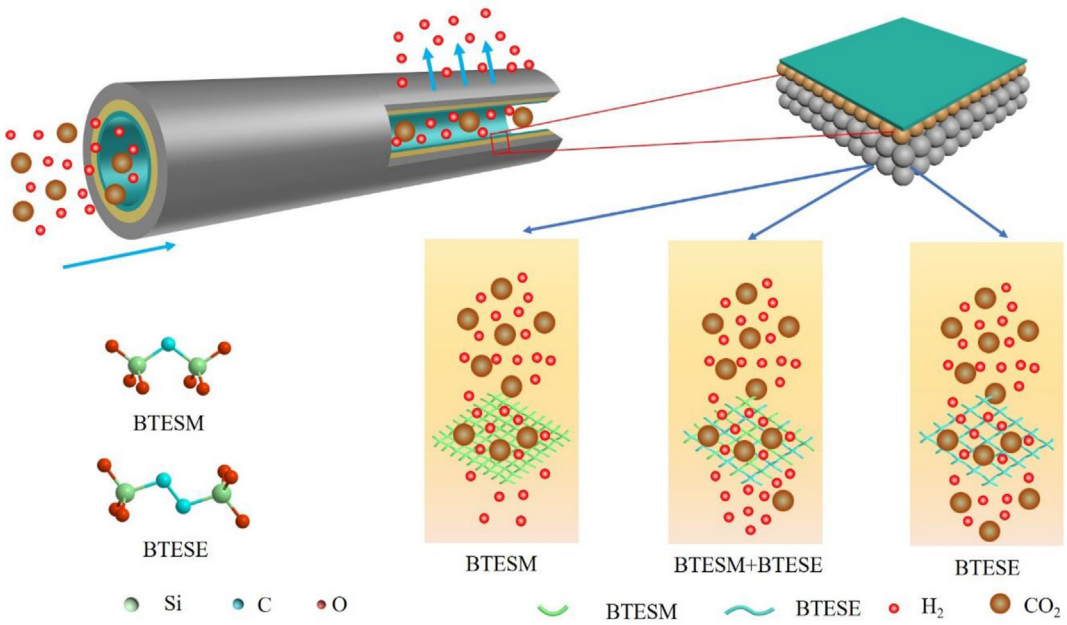

Fig. 10 – Schematic illustration of the hypothetical structures for BTESE-BTESM membranes for H_2/CO_2 separation.

of the membrane, while the H_2/CO_2 permselectivity is exceptionally low. The introduction of BTESM into the BTESE network confers BTESE-BTESM membranes with moderate microstructure. By tuning the ratio of BTESE to BTESM, the microstructure of the co-polymerization organosilica can be effectively adjusted. The E-M-3:7 membrane showed the optimal structure for H_2/CO_2 separation.

Fig. 11 compares the H_2/CO_2 separation performance of the co-polymerization BTESE-BTESM membranes with that of silica-based membranes [32,33], BTESE-derived membranes [34–36], co-polymerization organosilica membranes [21,23,24]), zeolite [37,38] and MOF [39–42] membranes. The detailed data of those membranes are presented in Table 2. Traditional SiO_2 membranes exhibited high H_2/CO_2 permselectivity, but its H_2 permeance is still low in comparison. In addition, SiO_2 membranes usually suffer from poor hydrothermal stability under steam conditions used for practical application. Compared with SiO_2 membranes, BTESE-derived membranes generally have enhanced hydrothermal stability but their H_2/CO_2 permselectivity is not satisfied. Although metal doping can improve the H_2/CO_2 permselectivity of BTESE membranes, the H_2 permeance is seriously decreased which presents a trade-off limitation. There are a few co-polymerization organosilica membranes reported for H_2/CO_2separation, however the performance is still under the upper bound limit of 2008. In addition, the performance of the zeolite and MOFs membranes were also presented in Fig. 11, which showed either a low H_2 permeance or a low H_2/CO_2 permselectivity. We observed that

Please cite this article as: Zhang H et al., Tuning the microstructure of organosilica membranes with improved gas permselectivity via the co-polymerization of 1,2-bis(triethoxysilyl)ethane and 1,2-bis(triethoxysilyl)methane, International Journal of Hydrogen Energy, https://doi.org/10.1016/j.ijhydene.2021.02.139

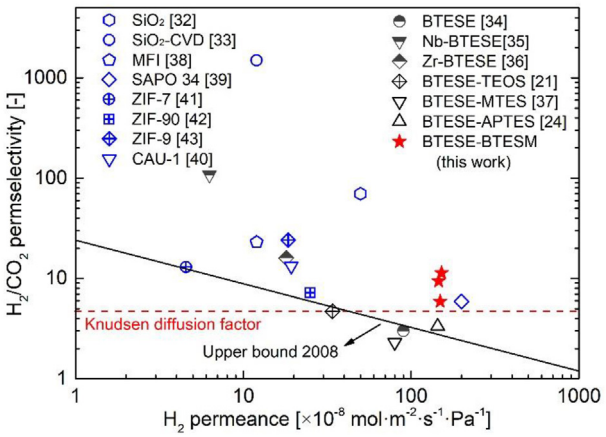

Fig. 11 – Comparison of H_2/CO_2 separation performance for BTESE-BTESM membranes prepared in this study with that of other membranes reported in the literatures (the upper bound 2008 line is drawn by conversing permeability to permeance assuming the membranes thickness of 100 nm).

the H_2/CO_2 separation performance of the as-prepared BTESE-BTESM membranes in this work are far above the upper bound limit of 2008, and the optimal membrane (i.e., E-M-3:7) showed a very competitive H_2/CO_2 separation performance compared with that of aforementioned membranes reported in the literatures. However, the performance of E-M-3:7 membrane is still far away from the requirements of industry (H_2 permeance>5 × 10^{-6} mol m^2 s^{-1}·Pa^{-1}, H_2/CO_2 permselectivity>30) [35]. In particular, to simultaneously improve the H_2/CO_2 permselectivity as well as the H_2 permeance is the objective of our future investigations.

Conclusions

Co-polymerization of BTESE-BTESM membranes were prepared by using the sol-gel method. The influences on the microstructure and gas separation performance were investigated by changing the molar ratios of BTESE to BTESM. As evident by chemical characterization, BTESM was successfully introduced into the BTESE network. According to the microstructural analysis, we found that the proportion of BTESM has significant influence on the resultant BTESE-BTESM networks. As the proportion of BTESM increased, the surface area, pore volume and pore size of BTESE-BTESM powders gradually decreased, which resulted in the decreased gas permeance of the corresponding BTESE-BTESM membranes. However, the introduction of BTESM has a slight impact when considering small gas (He and H_2) permeance, where large gas (CO_2, N_2, CH_4, and SF_6) has a sharp decline as the proportion of BTESM increased. Compared with the pure BTESE membrane, the gas permselectivity can be significantly improved by the co-polymerization of BTESE and BTESM. The E-M-3:7 membrane exhibited the highest H_2/CO_2 (11.3) and H_2/N_2 (26.8) permselectivity while remain a relatively high H_2 permeance of 1.52 × 10^{-6} mol m^2 s^{-1}·Pa^{-1}, which is considerably higher than the upper bound limit of 2008. This work may provide novel insights for designing and developing high-performance organosilica gas separation membranes by the co-polymerization method.

Table 2 – Comparison of as-prepared BTESE-BTESM membranes with other reported membranes in terms of H_2/CO_2 separation performance.

Membranes materials	Test temperature (°C)	H_2 permeance (mol·m^2·s^{-1}·Pa^{-1})	H_2/CO_2 permselectivity [–]	Ref.
SiO_2	200	5 × 10^{-7}	70	[32]
SiO_2-CVD[a]	600	1.2 × 10^{-7}	1500	[33]
MFI zeolite	500	1.2 × 10^{-7}	23	[37]
SAPO 34 zeolite	30	2 × 10^{-6}	5.88	[38]
ZIF-7	220	4.55 × 10^{-8}	13	[40]
ZIF-90	200	2.5 × 10^{-7}	7.2	[41]
ZIF-9	25	1.85 × 10^{-7}	24.2	[42]
CAU-1	25	1.93 × 10^{-7}	13.27	[39]
BTESE	200	9 × 10^{-7}	3	[34]
Nb-BTESE	200	6.28 × 10^{-8}	108	[35]
Zr-BTESE	200	4.78 × 10^{-8}	15	[36]
BTESE-TEOS	200	3.4 × 10^{-7}	4.7	[21]
BTESE-MTES	200	8 × 10^{-7}	2.3	[23]
BTESA-APTES	200	1.44 × 10^{-6}	3.34	[24]
E-M-8:2	200	1.49 × 10^{-6}	5.9	This work
E-M-5:5		1.46 × 10^{-6}	9.4	
E-M-3:7		1.52 × 10^{-6}	11.3	

[a] Silica membranes were prepared by the chemical vapor deposition technology (SiO_2-CVD).

Please cite this article as: Zhang H et al., Tuning the microstructure of organosilica membranes with improved gas permselectivity via the co-polymerization of 1,2-bis(triethoxysilyl)ethane and 1,2-bis(triethoxysilyl)methane, International Journal of Hydrogen Energy, https://doi.org/10.1016/j.ijhydene.2021.02.139

Declaration of competing interest

The authors declare that they have no known competing financial interests or personal relationships that could have appeared to influence the work reported in this paper.

Acknowledgments

This work is supported by the National Natural Science Foundation of China of China (21490581), China Petroleum & Chemical Corporation (317008-6) and Guangxi Innovation Driven Development Foundation (AA172204092).

REFERENCES

[1] Ren X, Tsuru T. Organosilica-based membranes in gas and liquid-phase separation. Membranes 2019;9:107.
[2] Castricum HL, Paradis GG, Mittelmeijer-Hazeleger MC, Kreiter R, Vente JF, ten Elshof JE. Tailoring the separation behavior of hybrid organosilica membranes by adjusting the structure of the organic bridging group. Adv Funct Mater 2011;21:2319–29.
[3] Dral AP, Elshof JET. Organic groups influencing microporosity in organosilicas. Microporous Mesoporous Mater 2018;267:267–73.
[4] Rimsza J, Deng L, Du J. Molecular dynamics simulations of nanoporous organosilicate glasses using Reactive Force Field (ReaxFF). J Non-Cryst Solids 2016;431:103–11.
[5] Iler KR. The Chemistry of silica. New York, USA: Wiley & Sons Inc; 1979.
[6] Campaniello J, Engelen CWR, Haije WG, Pex P, Vente JF. Long-term pervaporation performance of microporous methylated silica membranes. Chem Commun 2004;7:834–5.
[7] Kanezashi M, Yoneda Y, Nagasawa H, Tsuru T, Yamamoto K, Ohshita J. Gas permeation properties for organosilica membranes with different Si/C ratios and evaluation of microporous structures. AIChE J 2017;63:4491–8.
[8] Kanezashi M, Yada K, Yoshioka T, Tsuru T. Design of silica networks for development of highly permeable hydrogen separation membranes with hydrothermal stability. J Am Chem Soc 2009;131:414–5.
[9] Wang J, Kanezashi M, Yoshioka T, Tsuru T. Effect of calcination temperature on the PV dehydration performance of alcohol aqueous solutions through BTESE-derived silica membranes. J Membr Sci 2012;s 415–416:810–5.
[10] Xin Y, Meng L, Niimi T, Nagasawa H, Kanezashi M, Yoshioka T, et al. Network engineering of a BTESE membrane for improved gas performance via a novel pH-swing method. J Membr Sci 2016;511:219–27.
[11] Song H, Wei Y, Qi H. Tailoring pore structures to improve the permselectivity of organosilica membranes by tuning calcination parameters. J Mater Chem 2017;5:24657–66.
[12] Zhang H, Wei Y, Qi H. Palladium-niobium bimetallic doped organosilica membranes for H_2/CO_2 separation. Microporous Mesoporous Mater 2020;305:110279.
[13] Qureshi HF, Nijmeijer A, Winnubst L. Influence of sol-gel process parameters on the micro-structure and performance of hybrid silica membranes. J Membr Sci 2013;446:19–25.
[14] Li G, Niimi T, Kanezashi M, Yoshioka T, Tsuru T. Equilibrium shift of methylcyclohexane dehydrogenation in a thermally stable organosilica membrane reactor for high-purity hydrogen production. Int J Hydrogen Energy 2013;38:15302–6.
[15] Castricum HL, Kreiter R, Veen HMV, Blank DHA, Vente JF, Elshof JET. High-performance hybrid pervaporation membranes with superior hydrothermal and acid stability. J Membr Sci 2008;324:111–8.
[16] Castricum HL, Sah A, Kreiter R, Blank DH, Vente JF, ten Elshof JE. Hybrid ceramic nanosieves: stabilizing nanopores with organic links. Chem Commun 2008;9:1103–5.
[17] Zheng F-T, Yamamoto K, Kanezashi M, Tsuru T, Ohshita J. Preparation of bridged silica RO membranes from copolymerization of bis (triethoxysilyl) ethene/(hydroxymethyl) triethoxysilane. Effects of ethenylene-bridge enhancing water permeability. J Membr Sci 2018;546:173–8.
[18] Wu X, Liu H, Wei Y, Fei Y, Qi H. Negatively charged organic–inorganic hybrid silica nanofiltration membranes for lithium extraction. Chin J Chem Eng 2020;28:749–57.
[19] Song H, Wei Y, Wang C, Zhao S, Qi H. Tuning sol size to optimize organosilica membranes for gas separation. Chin J Chem Eng 2018;26:53–9.
[20] Chang K-S, Yoshioka T, Kanezashi M, Tsuru T, Tung K-L. A molecular dynamics simulation of a homogeneous organic-inorganic hybrid silica membrane. Chem Commun 2010;46:9140–2.
[21] Meng L, Kanezashi M, Wang J, Tsuru T. Permeation properties of BTESE-TEOS organosilica membranes and application to O_2/SO_2 gas separation. J Membr Sci 2015;496:211–8.
[22] Guo M, Kanezashi M, Nagasawa H, Yu L, Yamamoto K, Gunji T, et al. Fine-tuned, molecular-composite, organosilica membranes for highly efficient propylene/propane separation via suitable pore size. AIChE J 2020;66:e16850.
[23] Chai S, Du H, Zhao Y, Lin Y, Kong C, Chen L. Fabrication of highly selective organosilica membrane for gas separation by mixing bis(triethoxysilyl)ethane with methyltriethoxysilane. Separ Purif Technol 2019;222:162–7.
[24] Guo M, Kanezashi M, Nagasawa H, Yu L, Ohshita J, Tsuru T. Amino-decorated organosilica membranes for highly permeable CO_2 capture. J Membr Sci 2020;611:118328.
[25] Díaz-Benito B, Velasco F, Martínez F, Encinas N. Hydrolysis study of bis-1, 2-(triethoxysilyl) ethane silane by NMR. Colloids Surf, A 2010;369:53–6.
[26] Kappert EJ, Bouwmeester HJ, Benes NE, Nijmeijer A. Kinetic analysis of the thermal processing of silica and organosilica. J Phys Chem B 2014;118:5270–7.
[27] Ngamou PHT, Overbeek JP, Kreiter R, Veen HMV, Vente JF, Wienk IM, et al. Plasma-deposited hybrid silica membranes with a controlled retention of organic bridges. J Mater Chem 2013;1:5567–76.
[28] Al-Oweini R, El-Rassy H. Synthesis and characterization by FTIR spectroscopy of silica aerogels prepared using several $Si(OR)_4$ and $R''Si(OR')_3$ precursors. J Mol Struct 2009;919:140–5.
[29] Kanezashi M, Miyauchi S, Nagasawa H, Yoshioka T, Tsuru T. Gas permeation properties through Al-doped organosilica membranes with controlled network size. J Membr Sci 2014;466:246–52.
[30] Thommes M, Kaneko K, Neimark AV, Olivier JP, Rodriguez-Reinoso F, Rouquerol J, et al. Physisorption of gases, with special reference to the evaluation of surface area and pore size distribution (IUPAC Technical Report). Pure Appl Chem 2015;87:1051–69.
[31] Karakiliç P, Huiskes C, Luiten-Olieman MWJ, Nijmeijer A, Winnubst L. Sol-gel processed magnesium-doped silica membranes with improved H_2/CO_2 separation. J Membr Sci 2017;543:195–201.
[32] de Vos RM, Verweij H. High-selectivity, high-flux silica membranes for gas separation. Science 1998;279:1710–1.

Please cite this article as: Zhang H et al., Tuning the microstructure of organosilica membranes with improved gas permselectivity via the co-polymerization of 1,2-bis(triethoxysilyl)ethane and 1,2-bis(triethoxysilyl)methane, International Journal of Hydrogen Energy, https://doi.org/10.1016/j.ijhydene.2021.02.139

[33] Lee D, Zhang L, Oyama ST, Niu S, Saraf RF. Synthesis, characterization, and gas permeation properties of a hydrogen permeable silica membrane supported on porous alumina. J Membr Sci 2004;231:117–26.
[34] Moriyama N, Nagasawa H, Kanezashi M, Ito K, Tsuru T. Bis(triethoxysilyl)ethane (BTESE)-derived silica membranes: pore formation mechanism and gas permeation properties. J Sol Gel Sci Technol 2018;86:63–72.
[35] Qi H, Chen H, Li L, Zhu G, Xu N. Effect of Nb content on hydrothermal stability of a novel ethylene-bridged silsesquioxane molecular sieving membrane for H_2/CO_2 separation. J Membr Sci 2012;421–422:190–200.
[36] Hove MT, Nijmeijer A, Winnubst L. Facile synthesis of zirconia doped hybrid organic inorganic silica membranes. Separ Purif Technol 2015;147:372–8.
[37] Wang H, Dong X, Lin YS. Highly stable bilayer MFI zeolite membranes for high temperature hydrogen separation. J Membr Sci 2014;450:425–32.
[38] Das JK, Das N, Bandyopadhyay S. Highly selective SAPO 34 membrane on surface modified clay-alumina tubular support for H_2/CO_2 separation. Int J Hydrogen Energy 2012;37:10354–64.
[39] Zhou S, Zou X, Sun F, Ren H, Liu J, Zhang F, et al. Development of hydrogen-selective CAU-1 MOF membranes for hydrogen purification by 'dual-metal-source' approach. Int J Hydrogen Energy 2013;38:5338–47.
[40] Li Y, Liang F, Bux H, Yang W, Caro J. Zeolitic imidazolate framework ZIF-7 based molecular sieve membrane for hydrogen separation. J Membr Sci 2010;354:48–54.
[41] Huang A, Dou W, Caro Jr. Steam-stable zeolitic imidazolate framework ZIF-90 membrane with hydrogen selectivity through covalent functionalization. J Am Chem Soc 2010;132:15562–4.
[42] Liu J, Liu C, Huang A. Co-based zeolitic imidazolate framework ZIF-9 membranes prepared on α-Al_2O_3 tubes through covalent modification for hydrogen separation. Int J Hydrogen Energy 2020;45:703–11.

Please cite this article as: Zhang H et al., Tuning the microstructure of organosilica membranes with improved gas permselectivity via the co-polymerization of 1,2-bis(triethoxysilyl)ethane and 1,2-bis(triethoxysilyl)methane, International Journal of Hydrogen Energy, https://doi.org/10.1016/j.ijhydene.2021.02.139